International Journal of Engineering Trends and Technology
ISSN: 2231–5381 / https://doi.org/10.14445/22315381/IJETT-V73I8P129

Volume 73 Issue 8, 342-354, August 2025

Original Article

Active Power Management in PV-Based EVs Using Switched Quasi Z-Source Converter

A.A. Mohamed Faizal[1], M. Anish John Paul[2], L. Nisha Evangelin[3], P. Sabarish[4], K. Vijetha[5], T.R. Premila[6]

[1]*Department of Electrical and Electronics Engineering, V V College of Engineering, Tisaiyanvilai, India.*
[2]*Department of Electrical and Electronics Engineering, Mar Ephraem College of Engineering and Technology, Elavuvilai, Tamil Nadu, India.*
[3]*Department of Computer Science and Engineering, Noorul Islam Centre for Higher Education, Kanyakumari, Tamil Nadu, India.*
[4]*Department of Electrical and Electronics Engineering, K.Ramakrishnan College of Technology, Samayapuram, Trichy, Tamil Nadu, India.*
[5]*Department of Electrical Engineering, Medicaps University, Indore, India.*
[6]*Department of Electrical and Electronics Engineering, Vels Institute of Science Technology of Advanced Studies, Tamil Nadu, India.*

[1]*Corresponding Author : aamohamedfaizal106@gmail.com*

Received: 07 December 2024 Revised: 24 May 2025 Accepted: 23 August 2025 Published: 30 August 2025

Abstract - *The incorporation of Energy Storage Systems (ESS) has become vital in advanced power systems, especially with the enhancement of penetration of Renewable Energy Sources (RES) and rapid development of Electric Vehicles (EVs). Batteries are exploited among distinct ESS, because of their reliability, compact size and quick dynamic response, making them appropriate for grid-connected applications. Nevertheless, efficient battery incorporation requires advanced power conversion and management approaches. This research develops an innovative approach for improving power conversion efficacy and battery management in Photovoltaic (PV) related EV systems via a Switched Quasi Z-source (SQZSC) converter coupled with an active balancing circuit. The low voltage of the PV system is solved by the SQZSC converter to offer maximum voltage gain and efficacy. Moreover, a Maximum Power Point Tracking (MPPT) based on Radial Basis Function Networks (RBFNN) approach is utilized to assure effective power extraction in dynamic conditions. To regulate the delivery of power when no power is available from PV, a bidirectional battery balancing circuit is exploited that adapts the voltage level based on the battery state and is managed by a Proportional Integral (PI) controller. The implemented work is implemented in MATLAB/Simulink, the outcomes validate that the developed balancing approach achieves inferior switching loss in the equalization period , in addition to enhancing the performance of bidirectional battery equalization.*

Keywords - *Energy storage systems, RES, PV, Quasi Z-source converter, RBFNN-MPPT, Active balancing circuit, PI controller, MATLAB.*

1. Introduction

The wide usage of fossil fuels in internal combustion engine vehicles, such as those that run on gasoline, diesel, or Liquefied Petroleum Gas (LPG), raises serious environmental issues, especially when releasing greenhouse gases like CO2 [1]. Additionally, a significant obstacle facing the automotive sector is the global depletion of fossil fuels and the resulting increase in the price of crude oil [2]. When the electrical energy needed for EV charging comes from RES like solar power, EVs are a clean and green alternative to the current transportation system [3-7]. The voltage generated from the PV is low due to the ecological changes, which necessitate the DC-DC converter [8] topology for boosting the voltage. Different conventional converters, like the Boost converter [9], can enhance the input voltage to a higher level. Nevertheless, it has high output voltage ripple and poor performance under heavy load, particularly at a large duty cycle. The Luo converter is developed in [10] and provides maximum voltage gain with the aid of energy-transferring capacitors and inductors. However, it has enhanced complexity because of multiple energy storage elements. Then, the SEPIC converter [11] offers the capability to both step down and step up voltage and diminishes the current ripple on the input side. Nevertheless, it is less efficient because of its higher switching and conduction losses. The Z-source converter [12] offers inherent shoot-through protection for the inverter bridge. Nevertheless, it has a larger size, higher cost, and enhanced component count.

Therefore, the Switched Quasi Z-source converter is utilized to proficiently raise the low and changing output voltage from the PV system, offering maximum voltage gain and continuous input current, thereby addressing the inadequacies of conventional converters. On the other hand, the MPPT methods [13] are incorporated to extract optimal power from the PV system. The conventional MPPT topologies, like Fuzzy-MPPT [14], function well under varying environmental conditions and offer a fast dynamic response. However, it is not able to attain optimal performance under all temperature and irradiance conditions. An ANN-MPPT [15] has the capability to approximate nonlinear relationships among input parameters and MPP.

Nevertheless, it has implementation complexity, a higher computational load and needs a large training dataset. Then, the ANFIS-MPPT [16] offers strong adaptability and fast convergence towards the global MPP, particularly in the occurrence of partial shading. However, it has high computational complexity and a necessity for a large training dataset. These algorithms have oscillations at the location of the highest power at lower irradiance values, which makes it harder to estimate high power and lowers the SPV module's power transformation efficiency [17-19]. Moreover, most NN-based methods require all training data to be used as hidden layer neurons, resulting in increased complexity and more computation time [20]. Thus, the RBFNN-MPPT algorithm is implemented to outperform the conventional approaches by offering improved tracking efficiency, faster convergence, and minimal power oscillations near the MPP, especially under partial shading conditions.

Battery Energy Storage Systems (BESS) are crucial for supplying off-grid electricity at night and on overcast days. Thus, high-specific energy and power storage systems are needed in RES and automotive systems in order to store the energy [21]. Various battery technologies, comprising nickel metal hydride (Ni-MH), lithium-ion (Li-ion), nickel-cadmium (Ni-Cd), lead acid and sodium-sulfur (Na-S) are utilized in EVs [22]. Compared to other batteries, Li-ion batteries have a better specific energy, energy density, and specific power characteristics, making them a viable energy storage technology used in this developed work. Single Li-ion battery cells only deliver a maximum voltage of 4.2 V, which is insufficient for EV applications. To achieve the voltage requirements of EVs, many cells are connected in series [23]. Number of cells in the battery pack increases, inter-cell inconsistency becomes an inevitable issue that worsens with subsequent cycles of charge and discharge. Throughout the battery pack, this initial imbalance is caused by an inevitable irregularity [24].To solve these issues, a Battery Management System (BMS), which combines control and management components, is necessary to ensure that every cell in the battery pack operates in an optimal manner. A great deal of balancing circuits have been researched in the last few years [25]. This is classified into 2 groups: passive and active. Although passive balancing is easy to develop and install and quite inexpensive, its inherent energy loss makes it less desirable from an energy-saving perspective [26, 27]. Therefore, the implemented topology is integrated with the active balance circuit, which uses a bi-directional balancing circuit in this work for charging or discharging based on the Battery's needs.

1.1. Research Gap

Conventional converters often have difficulties like higher component stress, maximum output voltage ripple, enhanced conduction losses and inadequate voltage gain under low irradiance conditions. A novel Switched Quasi Z-source converter solves this. Furthermore, the intelligent MPPT algorithms have enhanced tracking abilities, but they are susceptible to power oscillations near the MPP, leading to diminished tracking efficiency, which is resolved by a developed RBFNN-MPPT controller. As the number of series-linked Li-ion cells increases, there is a risk of imbalance in SOC that degrades the life of the Battery and the reliability of the system. Though numerous battery equalization approaches exist, passive approaches waste the energy as heat and lack scalability, while the active approaches, particularly bidirectional balancing circuits, are underexplored in real-time SOC management for PV-EV applications.

The following describes the proposed topology's contribution:

- Switched Quasi Z-source converter for improving the low voltage obtained from the PV system
- RBFNN-based MPPT topology is utilized for tracking optimal power from the PV system
- To expand the battery pack's usable capacity and enable it to function at its anticipated performance level, a bidirectional voltage balancing circuit is developed.

2. Proposed Modelling

With the goal of lowering dependency on fossil fuels utilized in conventional heat generation, PV is widely employed as a dependable, affordable, and sustainable RES. BESS are crucial for supplying off-grid electricity at night and on overcast days. Henceforth, the proposed work incorporates a Switched Quasi Z-source converter for an active balancing circuit in PV-based EV applications. The block diagram of the developed work is presented in Figure 1, which is defined as follows.

Adopting a high efficiency and voltage gain Switched Quasi Z-source converter increases the voltage from the PV system. An optimal power is extracted by utilizing the RBFNN MPPT topology. The PWM generator receives the regulated output voltage and current and produces the required pulses for the Switched Quazi Z-source converter to function more effectively. The enhanced and controlled voltage is distributed to the load applications.

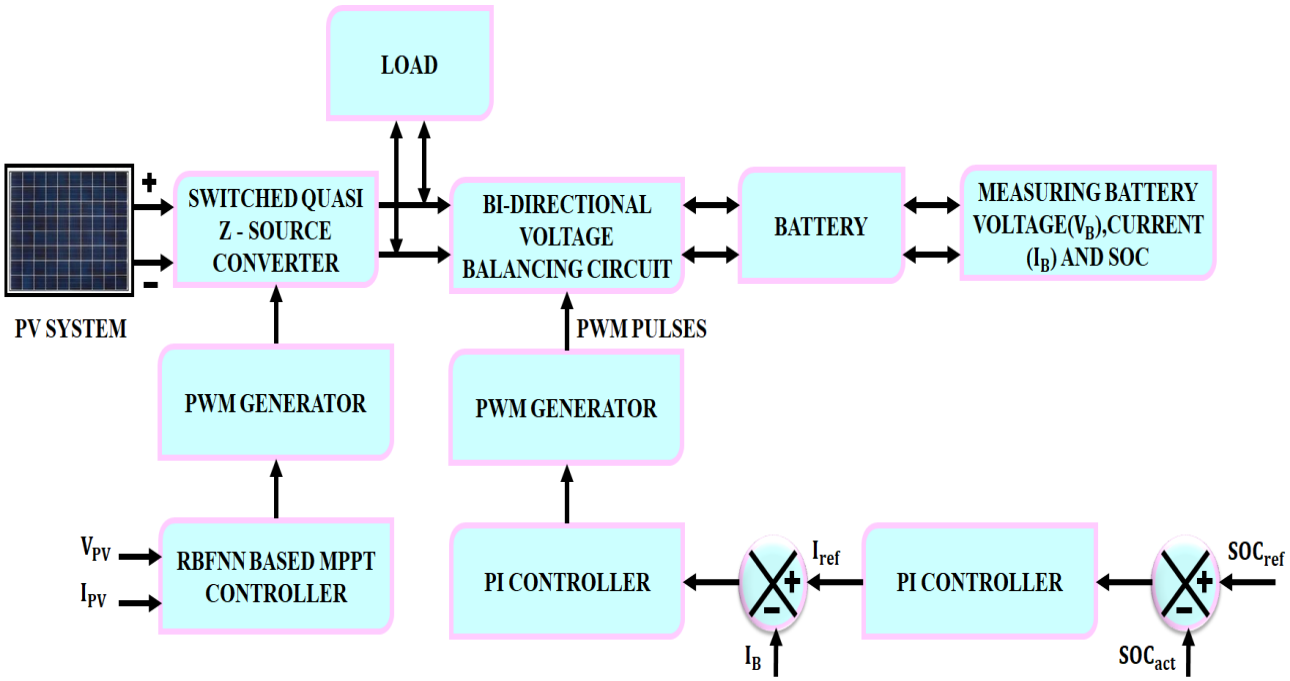

Fig. 1 Block diagram for the proposed work

Furthermore, BESS is applied to supply off-grid electricity during the lagging energy from the PV system. A bidirectional voltage balancing circuit is provided to buck/boost the voltage per the battery condition, delivering power to the battery system to store energy. Meanwhile, the Battery's current, voltage, and SOC are measured to distribute the energy constantly. When an error signal is generated, SOC_{act} is compared to SOC_{ref} And supplied to the PI controller for error compensation. From that, an actual current I_B It has been developed, which is compared with I_{ref} The error signal is obtained and delivered to the PI controller to generate the controlled output voltage for the PWM generator.

The pulses are generated by a PWM generator for better operation of the Bidirectional balancing circuit, and an uninterruptible power supply is distributed to the load system. By enhancing power extraction efficacy and diminishing energy losses, the developed system lowers the energy costs. Furthermore, improved battery lifespan via active SOC balancing diminishes replacement frequency, diminishing long-term maintenance costs. The upfront cost is justified by considerable operational savings and enhanced system reliability in EV-PV applications.

The developed research provides long-term benefits by improving PV-based EV systems' reliability, efficacy and sustainability. It assures optimal energy extraction, extended battery life and stable power delivery, diminishing reliance on grid electricity and carbon emissions. It aids in the diminished fossil fuel dependency, clean energy transition, and development of smart transportation systems, thereby enhancing the environmental and societal impact.

2.1. Modelling of PV System

The power provided by PV panels is controlled by the arrangement of parallel or series-connected solar cells. Double-diode and single-diode modules are the two main categories of PV cells. Despite the great precision of double-diode modules, the structural complexity is shown to cause low analytical speed. Conversely, because of their exceptional precision, single-diode modules are extensively used in many power applications. Consequently, the single diode-based PV module that consists of a diode D, current source (I_{sc}), and parallel and series resistors R_{sh} , R_s Is the subject of this research. The output current (I_{PV}) is expressed by Kirchhoff's Current Law using Figure 2 as follows:

$$I_{PV} = n_p I_L - I_D - \frac{V_D}{R_{sh}} \quad (1)$$

Where n_p The number of parallel linked cells is, R_{sh} is the shunt resistance, I_D Is the diode current, I_L specifies light-generated current and V_D Is the diode voltage? The following Equation (2) can be used to compute diode current:

$$I_D = n_p I_{OS} \left[exp \left(\frac{q(V + I_{RS})}{n_S AKT} \right) - 1 \right] \quad (2)$$

Here, q specifies the electron charge, I_{OS} indicates the reverse saturation current, n_s Denotes the series-connected cells, AKT specifies the Boltzmann constant temperature and kelvin, V represents the output voltage, and R_s Denotes the series resistance. To increase the low voltage from the PV system with excellent efficiency and voltage gain, the Switched Qazi Z-Source converter is developed in this work, as shown in the following illustration.

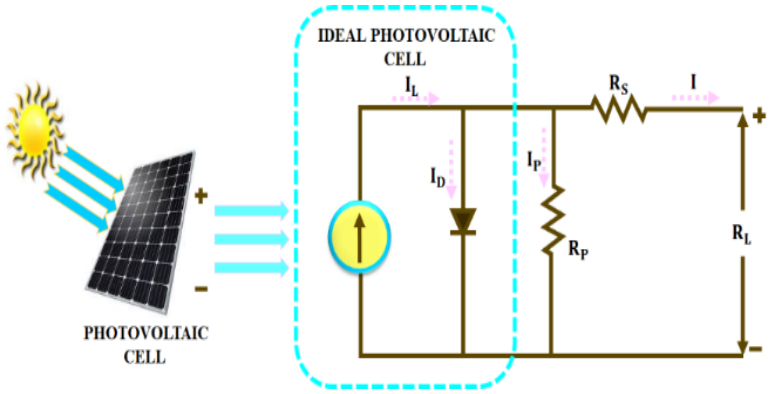

Fig. 2 Configuration of PV cell

2.2. Modelling of SQZSC Converter

Figure 3 illustrates the proposed SQZSCs' circuit layout, which functions in both discontinuous and continuous current modes (CCM and DCM). It has 3 diodes, 3 capacitors, 2 inductors and 2 switches respectively. The proposed converter has operated in 4 modes, which are expressed as follows,

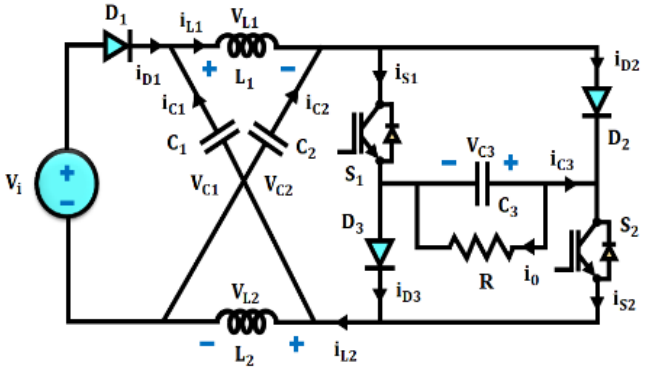

Fig. 3 Circuit diagram for the proposed Switched Quasi Z-source converter

2.2.1. Mode 1 $[t_0, t_1]$

In this state, diodes D_1, D_2 and D_3 are reverse biased, indicating that $iD_1 = iD_2 = iD_3 = 0$, while switches S_1 and S_2 are simultaneously turned ON. Capacitors C_1, C_2 and C_3 are discharged, inductors L_1 and L_2 We are storing the energy in a capacitor. C_3 transfers that energy to the load. Figure 4(a) specifies that the current loop shows that the switches $iS_1 = iS_2$, capacitor C_1 has a similar current with an inductor L_1, i.e., $iC_1 = iL_1$ and capacitor C_2 has the same current as the inductor L_2, i.e., $iC_2 = iL_2$ In state 1, the following formulas are obtained.

$$\begin{cases} i_{S1} = i_{L1} + i_{L2} \\ i_{C3} = i_{S1} + i_o \end{cases} \tag{3}$$

$$\begin{cases} v_{L1} = v_{C1} + v_{C3} \\ v_{L2} = v_{C2} + v_{C3} \end{cases} \tag{4}$$

2.2.2. Mode 2 $[t_1, t_2]$

In this state, diodes D_1, D_2 and D_3 are forward conducted, switches S_1 and S_2 are turned OFF simultaneously, so that $iS_1 = iS_2 = 0$. Energy is released to the capacitor C_1 by input source V_i and inductor L_2; energy is released to the capacitor C_2 by input source V_i and two inductors L_1 and L_2; Input voltage source V_i releases energy to load and C_3 and L_1 and L_2. Since diodes D_1, D_2 contain the same current, as seen from the current loop in Figure 4(b), which has

$$\begin{cases} i_{D1} = i_{L1} - i_{C1} \\ i_{D2} = i_{L1} + i_{C2} \\ i_{D3} = i_o - i_{C3} \end{cases} \tag{5}$$

According to KVL, acquiring the voltage across the three capacitors in this position is possible.

$$\begin{cases} v_{C1} = V_i - v_{L2} \\ v_{C2} = V_i + v_{L1} \\ v_{C3} = V_i - v_{L1} - v_{L2} \end{cases} \tag{6}$$

Under both conditions, the resulting formulae may be obtained from the standpoint of the equilibrium of the Z-source network.

$$\begin{cases} i_{L1} = i_{L2} v_{C1} = v_{L2} \\ i_{C1} = i_{C2} v_{C1} = v_{C2} \end{cases} \tag{7}$$

2.2.3. Mode 3 $[t_2, t_3]$

While the current interactions between the components change, the voltage relationships remain the same as in State 2, as illustrated in Figure 4(c).

$$\begin{cases} i_{D1} = i_{L1} - i_{C1} i_{L1} = i_{L2} \\ i_{D2} = i_{L1} + i_{C2} i_{C1} = i_{C2} \\ i_{D3} = i_o - i_{C3} \end{cases} \quad (8)$$

2.2.4. Mode 4 $[t_3, t_4]$

The S1 and S2 remain in the off position. In this state, as opposed to States 2 and 3, the diodes D_1,D_2 and D_3 They are reverse-biased. As a result, voltages across capacitors C_1,C_2 stay the same as specified in Figure 4(d).

$$\begin{cases} i_{D1} = i_{L1} - i_{C1} i_{L1} = i_{L2} \\ i_{D2} = i_{L1} + i_{C2} i_{C1} = i_{C2} \\ i_{D3} = i_o - i_{C3} \end{cases} \quad (9)$$

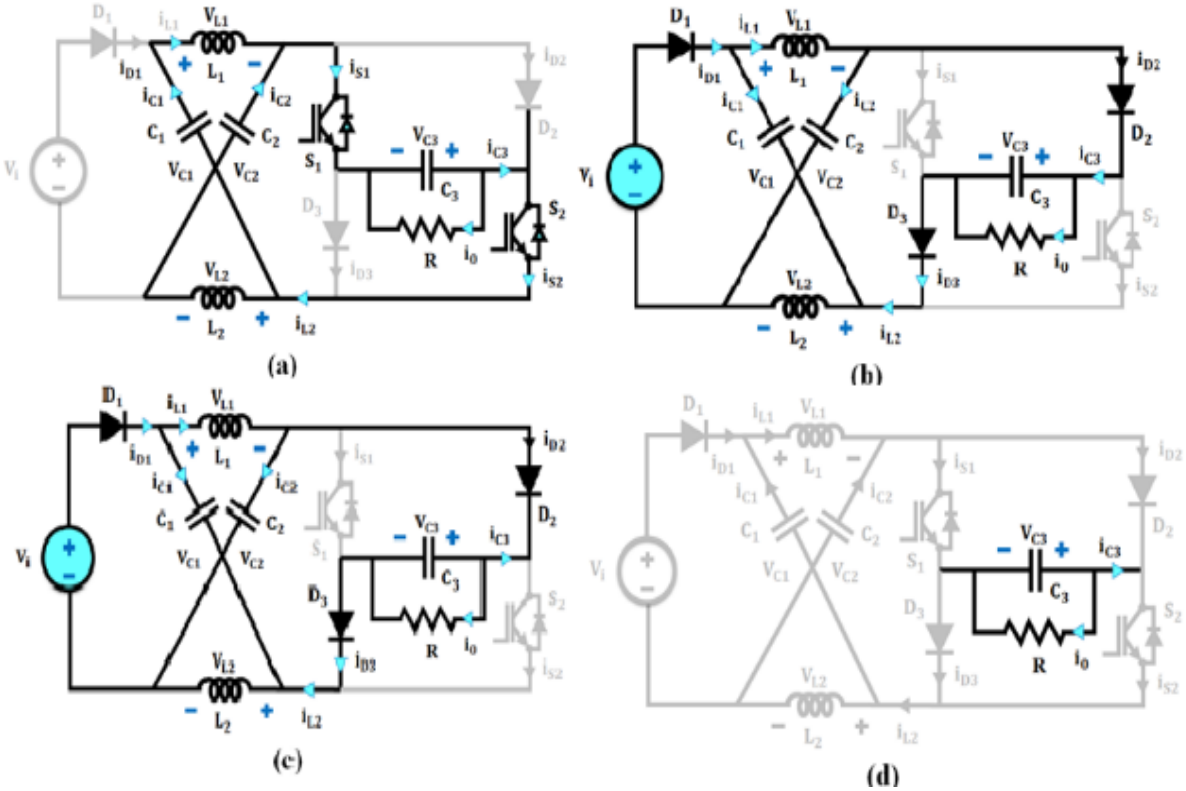

Fig. 4 Modes of operation (a) Stage 1, (b) Stage 2, (c) Stage 3, and (d) Stage 4.

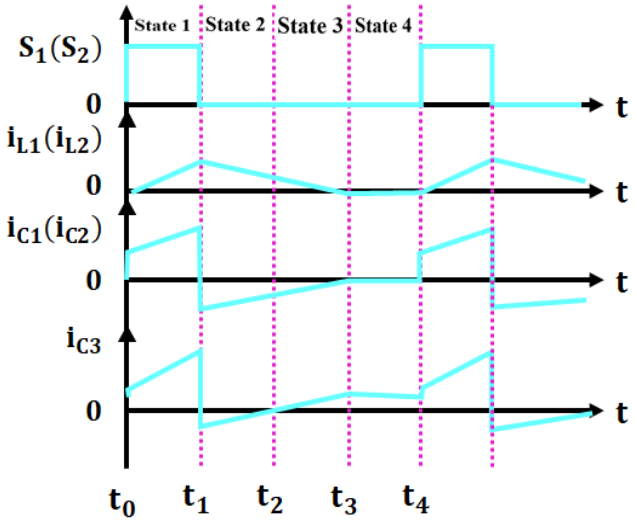

Fig. 5 Waveform of the proposed converter

The best power extraction method from the PV system is then achieved by the development of the RBFNN-based MPPT technology, which is explained below.

2.3. Modelling of RBFNN-Based MPPT

In Figure 6, the RBFNN is displayed. The Gaussian activation function that makes up the hidden layer has a vector at its centre in feature space. There are no weights between the input layer and the hidden layer. Every jj −th Gaussian hidden unit receives input layer straight from the source. RBF's $kkth$ unit output is provided as follows:

$$O_K = B_O + \sum_{j=1}^{h} w_{jk} * H_j \quad (10)$$

Where H_j Indicates radial basis output of jth hidden unit is denoted as $H_j = f(\left|\left|I - C_j\right|\right|)$, $c \in R$ belongs to center of RBF, which contains radius r.

$$f(x) = e^{\frac{-(\left|\left|I_i - C_j\right|\right|)^{\wedge 2}}{r^2}} \quad (11)$$

Here, $x_i = f(\left|\left|I_i - C_j\right|\right|)$ and $f(x)$ Is the Gaussian function equation? The technique most frequently used to update the centre C_{ij} and w_{jk} It is gradient descent learning. The neural network's performance is measured by Mean Square Error (MSE). According to target vector T and input I, the output-layer weights w_{jk} They are modified to lower the MSE, which is then given as,

$$E = \frac{1}{m}\sum_{k=1}^{m}(T_k - O_K)^2 \quad (12)$$

Here, T_k denotes output of the target network at the kth sample, O_K Represents the network output at the kth sample, and m specifies the total training patterns.

The battery system topology is developed to store excess energy from the PV system and is used during the lagging period of energy from PV. The bidirectional voltage balancing circuit is utilized to balance the voltage, which is illustrated as follows.

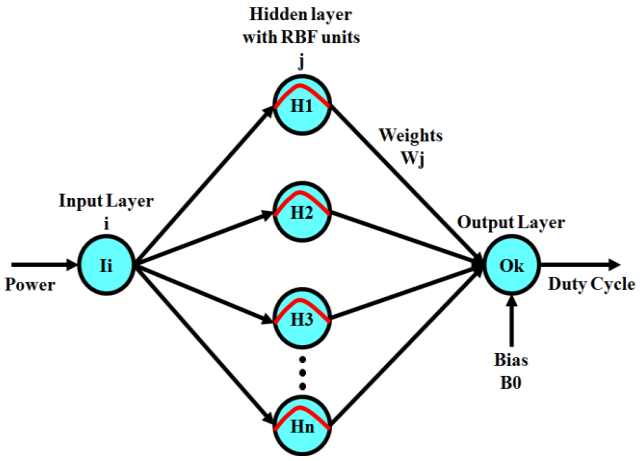

Fig. 6 Structure of RBFNN

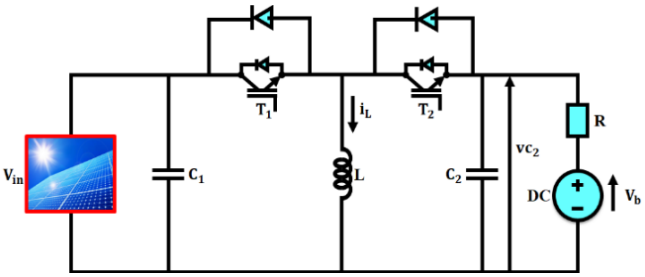

Fig. 7 Equivalent circuit diagram for the Bidirectional converter

2.4. Modelling of Bidirectional Voltage Balancing Circuit

The Bi-directional converter, which resides in the front part of the balancer, converts DC voltage. When voltage oscillation happens on the input voltage side of this voltage balancer, the converter maintains the consistency of the load voltage and lessens its impact. Because the DC converter can offer bi-directional energy flow, this voltage balancer, known as a Buck/Boost, is used as a transform balanced interface for active devices. Figure 7 displays the corresponding circuit diagram for modelling analysis.

The power electronic switches T_1 have a duty cycle of d_1. The load side analysis applies Thevenin's equivalent theory, which yields the equivalent resistance as well as voltage of R and v_b, as depicted in Figure 7. The capacitor voltage of C_1 is not chosen as a state variable because of the problematic loop topology. Thus, the state variables have been chosen in the following manner:

$$x_1(t) = \begin{bmatrix} i_L(t) \\ v_{c2}(t) \end{bmatrix} \quad (13)$$

$$u_1(t) = \begin{bmatrix} v_{in}(t) \\ v_b(t) \end{bmatrix} \quad (14)$$

Choose the load side voltage $v_{c2}(t)$ as the output variable by explicitly selecting an inductor current $i_L(t)$ and capacitor voltage of C_2:

$$y_1(t) = \begin{bmatrix} i_L(t) \\ v_{c2}(t) \end{bmatrix} \quad (15)$$

Maintaining a consistent supply voltage for the load and balancing voltage between the positive and negative rails are the two main functions of the voltage balancer portion. Because of the Buck/Boost converter part's steady-state gearbox ratio,

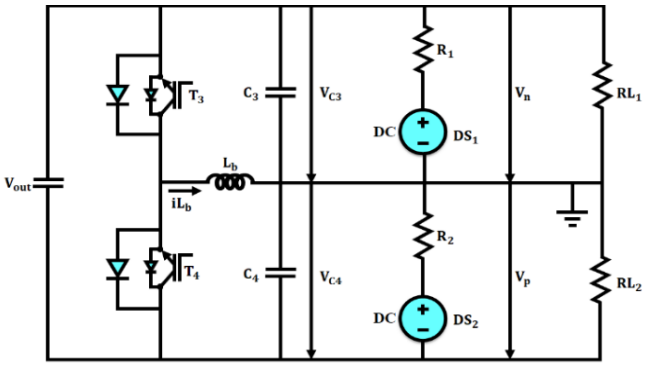

Fig. 8 Diagram for the voltage balancer part

The bidirectional Buck/Boost converter part's input and output voltage polarities were discovered to be inverted; as a result, the DC voltage balancer part's polarity has to be changed. In Figure 8, the corresponding circuit schematic for modelling analysis is displayed. $V_{out} = -VC_2$ This figure depicts the structure that is equivalent to the load side. The capacitor voltage of C_4 It is not chosen as a state variable in this structure because of the problematic loop topology. Thus, the state variables are chosen in the following manner:

$$x_2(t) = \begin{bmatrix} i_{Lb}(t) \\ v_{c3}(t) \end{bmatrix} \quad (16)$$

The input variables,

$$u_2(t) = \begin{bmatrix} V_{out}(t) \\ V_{DS1}(t) \\ V_{C4}(t) \end{bmatrix} \quad (17)$$

Following that, choose the following as the output variable: the inductor current $i_{Lb}(t)$, The capacitor voltages of C_3 and C_4 $v_{c3}(t)$ and $V_{C4}(t)$, the negative rail and positive rail voltages $V_n(t)$ and $V_p(t)$. Incorporating a bidirectional active balancing circuit improves battery lifespan and operational efficiency.

By constantly equalizing the SOC between all series-connected Li-ion cells, the system averts overcharging and deep discharging of separate cells. The uniform charge distribution lessens thermal stress and aging incongruities in the Battery. Furthermore, energy that would otherwise be lost in passive balancing is effectively preserved and redistributed, improving the overall energy exploitation. As a consequence, the Battery functions nearer to its rated capacity, ensuring prolonged service life and enhanced system reliability.

3. Results and Discussion

This research describes a method for the analysis of a quasi-Z-source converter with an active balancing circuit in PV-based EV applications. High voltage with high efficiency and voltage gain is attained by the developed Quasi Z-source converter, and the optimal power is effectively tracked with the aid of RBFNN-based MPPT topology.

Moreover, the Battery balancing bidirectional converter efficiency balances the voltage, and the constant power is dispersed to the load applications. The proposed system is fully implemented in MATLAB/Simulink, and an analysis with conventional techniques is provided to demonstrate the efficiency of the developed approach. The results are presented as follows, with parameter specifications detailed in Table 1.

Table 1. Parameter specification

Parameters	Specification
PV system	
No. of Panels	**20 panels**
Series connected solar PV	**36**
Peak power	**10 kW**
Short circuit voltage	**12V**
Open circuit voltage cells	**22.6V**
Switched Quasi Z-source converter	
$\mathbf{C_1, C_1}$	**4.7µF**
$\mathbf{C_0}$	2200 **µF**
$\mathbf{L_1, L_2}$	**1mH**
Switching frequency **f**	**10kHz**

Figure 9 shows the temperature and radiation waveform of a solar panel. It exhibits that the temperature fluctuates at first and then steadily maintains at 35°C for 0.25 seconds, as demonstrated in Figure 9(a). Figure 9(b) represents the irradiation oscillating during a certain period, after 0.25s, and then sustained steady at $1000(w/sq.m)$ respectively. These characteristics are exploited to simulate environmental variations influencing PV system performance, enabling assessment of MPPT and the response of the converter under dynamic conditions. Figure 10 demonstrates the solar panel waveform for Current and Voltage. It is clear from the result that the voltage fluctuates before gradually stabilizing at 60V after 0.25 seconds, as shown in Figure 10(a). Similarly, the solar panel current is suddenly raised and fluctuates for a certain period of time, after $0.25s$ it remained constant at 150A. As mentioned in Figure 10(b). These dynamic responses are associated with variations in irradiance and temperature conditions, assuring the efficacy of the MPPT and converter in adapting to environmental changes. Figure 11 displays the waveform of the converter's output current and voltage. Analysis reveals that voltage is initially quite high and varies, but eventually stabilizes at 400V as seen in Figure 11(a). Similarly, Figure 11(b) specifies that the current initially varies after 0.3s and remains constant at 8A. It reveals that the converter offers stable and managed outcomes, validating the robustness of the developed control approach in changing input conditions.

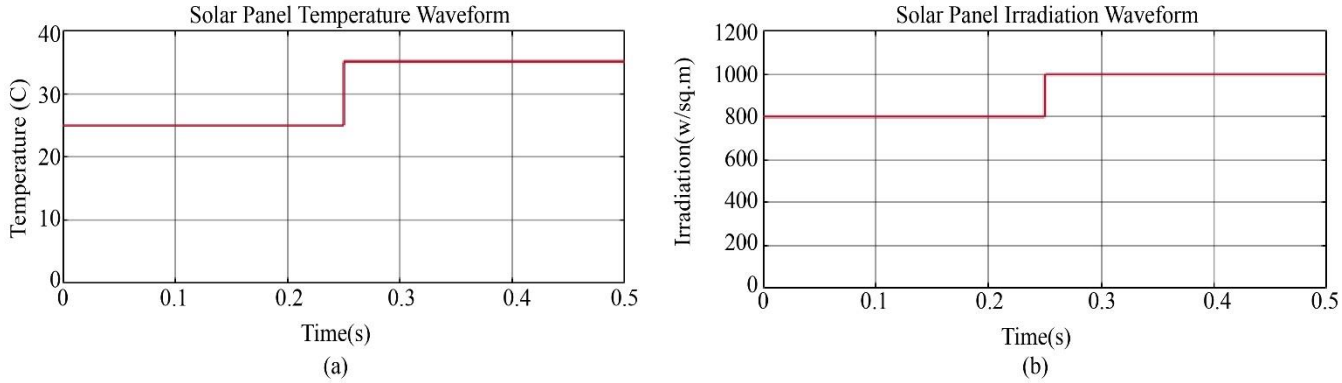

Fig. 9 Solar panel characteristics for (a) Temperature, and (b) Irradiation.

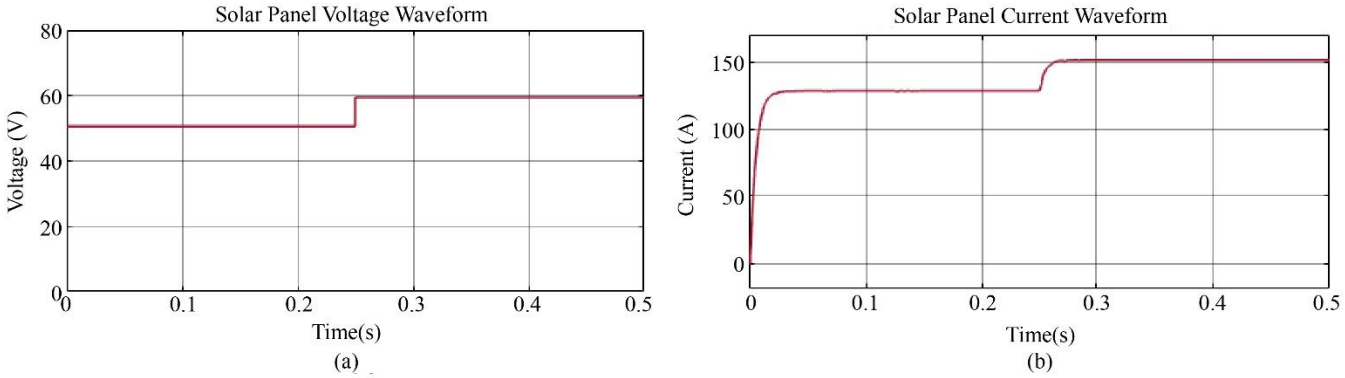

Fig. 10 Solar panel waveform for (a) Voltage, and (b) Current.

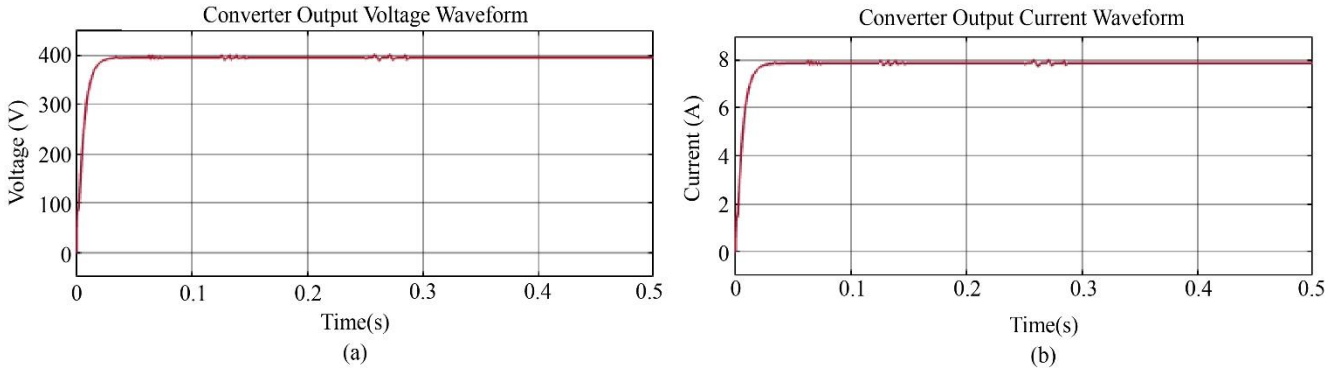

Fig. 11 Converter output waveform for (a) Voltage, and (b) Current.

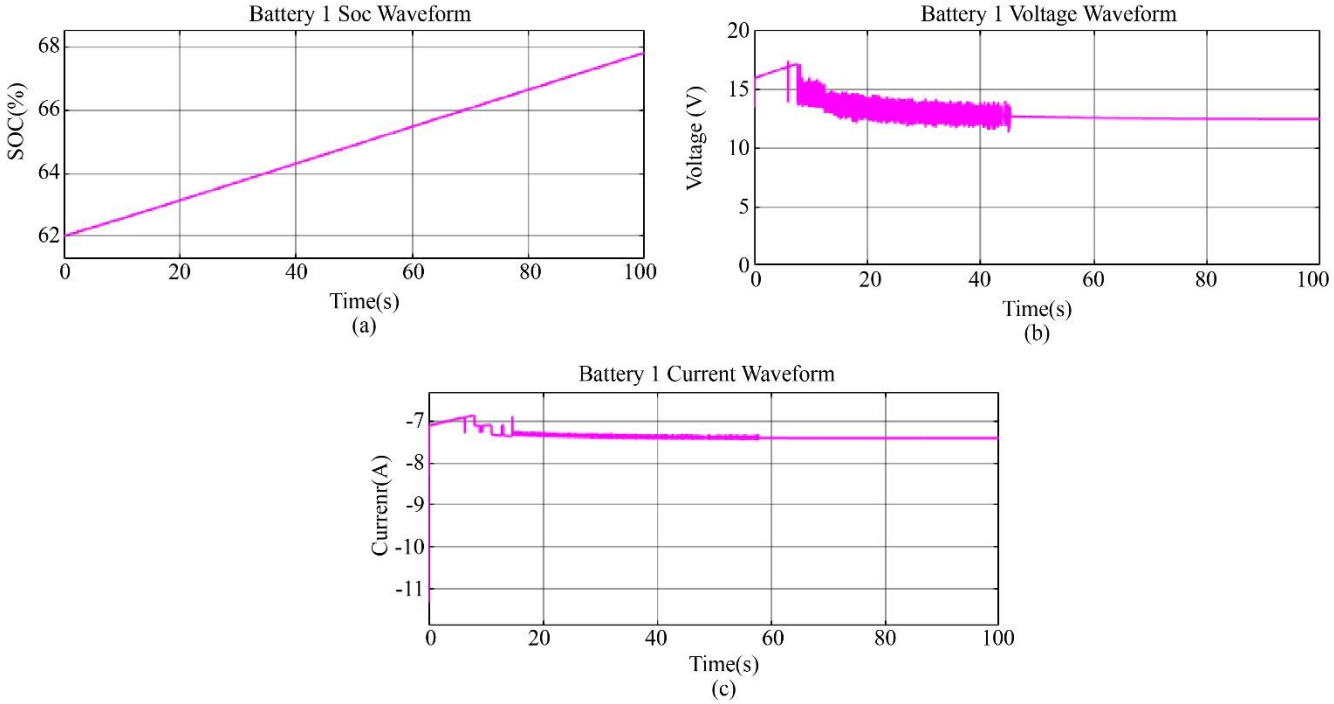

Fig. 12 Waveform Battery 1 (a) SOC, (b) voltage, and (c) Current.

Figure 12 shows Battery 1 waveform for SOC, voltage and current. As specified in Figure 12 (a), Battery 1 gradually increases its SOC and gets charged up to 65-70%. The voltage of battery 1 fluctuated initially after 60s, and it gradually

continued its persistent voltage at 12.5V as indicated in Figure 12 (b). Similarly, the Battery's current oscillated initially at a certain period, but after the 60s, it gradually maintained its constant current at -6A, as illustrated in Figure 12 (c). It indicates efficient and steady function of battery charging. Figure 13 displays the current, voltage and SOC waveform for Battery 2. The result shows that Battery 2 gradually increases its SOC and gets charged up to 65-70% as specified in Figure 13(a). In Figure 13 (b), the Battery's voltage fluctuated during the initial period of time, and it constantly maintained its voltage at 25 after 60s. Likewise, Figure 13 (c) shows that the Battery's current oscillated heavily in the initial time, after 60s it gradually maintained its current -8A, replicating organized charging after early transients.

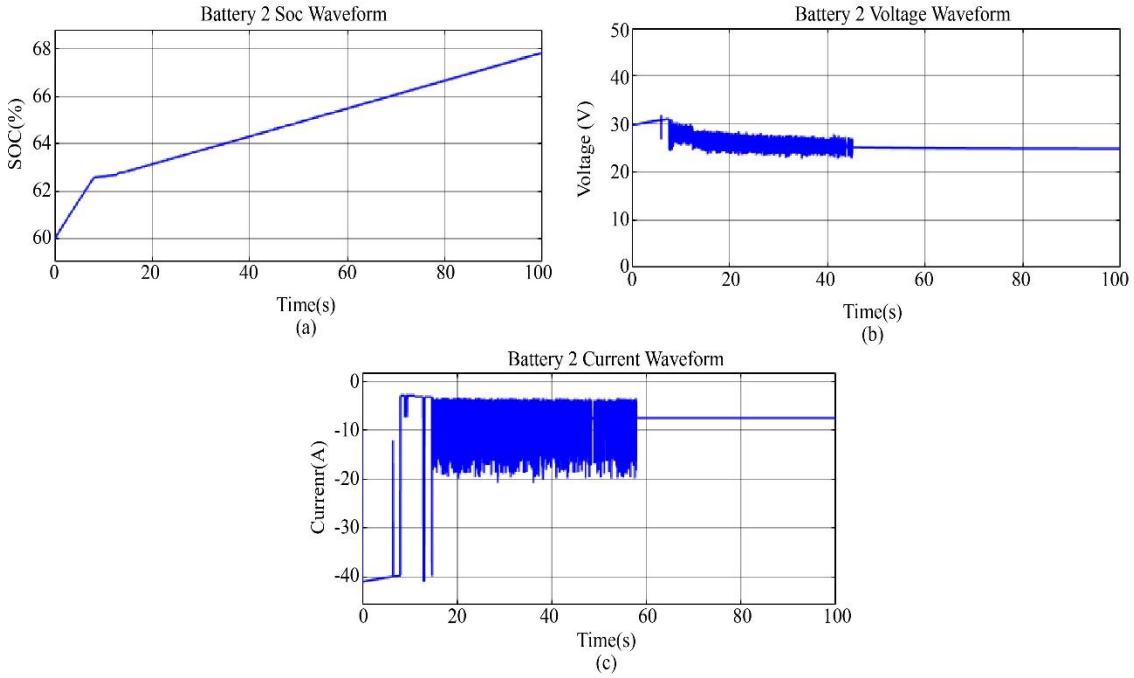

Fig. 13 Waveform Battery 2 (a) SOC, (b) Voltage, and (c) Current.

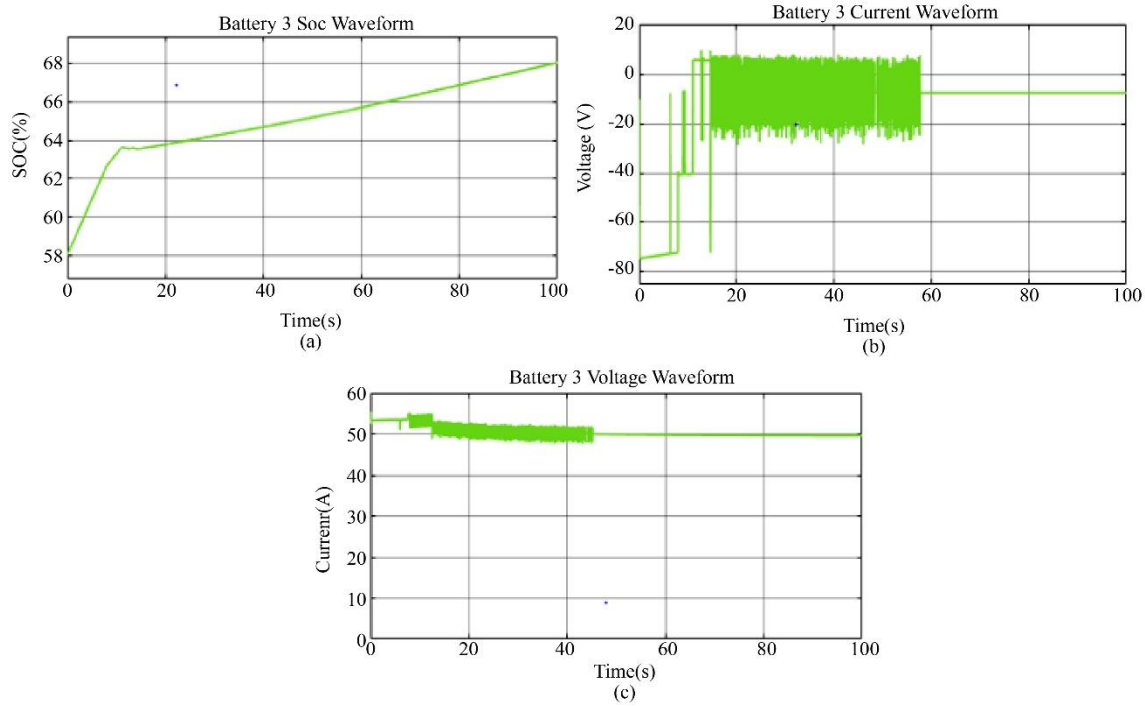

Fig. 14 Waveform Battery 3 (a) SOC, (b) Current, and (c) Voltage.

Figure 14 shows Battery 3 waveform for SOC, voltage and current, which shows that Battery 3 gradually increases its SOC and gets charged up to 65-70% as indicated in Figure 14(a). Moreover, as specified in Figure 14 (b), the current is highly raised and oscillates initially at a certain time, but after the 60s, the current remains constant at -8A. As illustrated in Figure 14 (c), voltage initially fluctuates slightly, and after 50s, it is constantly maintained at 50V. It assures steady charging behavior after primary oscillations. Figure 15 shows the 4 waveforms of the Battery for SOC, current, and voltage. Figure 15 (a) depicts that battery 4 gradually increased its SOC and was charged up to 65-70%. Similarly, the Battery's current is oscillated initially at certain period, after 40s it gradually sustained its stable current at -7A as illustrated in Figure 15 (b) respectively. Figure 15 (c) shows that battery 4's voltage is kept constant at 63V.

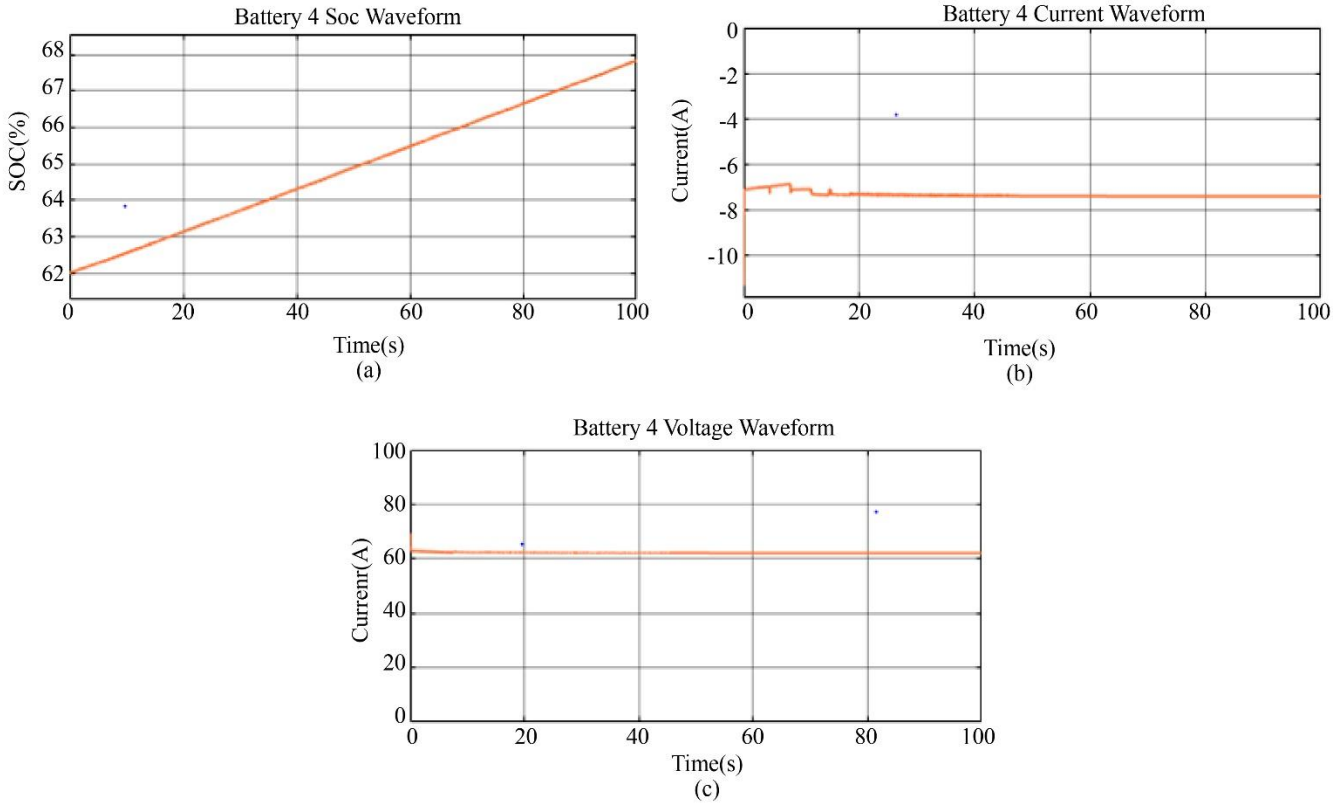

Fig. 15 Waveform for battery 4 (a) SOC, (b) current, and (c) voltage.

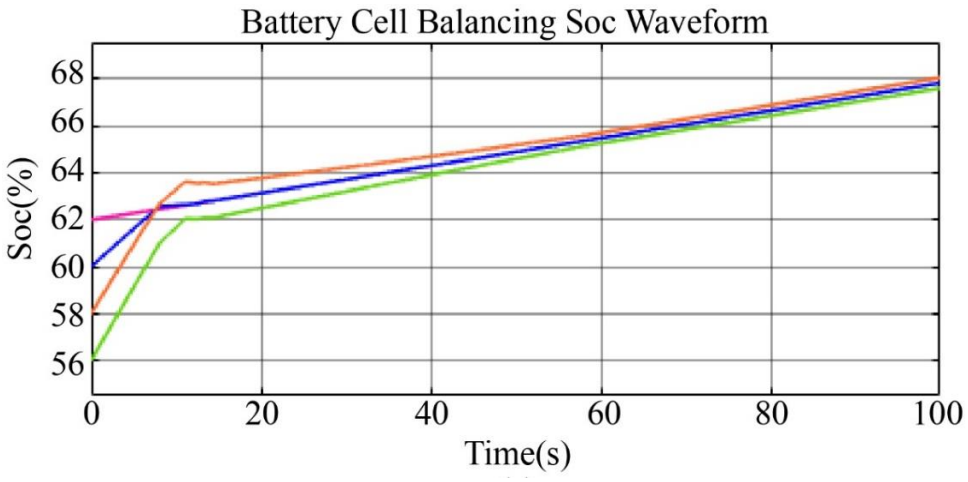

Fig. 16 Battery cell balancing SOC waveform

The SOC waveform for battery cell balancing is illustrated in Figure 16. Based on the examination of the data, it is seen that batteries 1, 2, 3 and 4 all have varying SOCs at first, and that all four batteries eventually balance at 70%, as shown in Figure 16. It validates the efficacy of the developed active balancing approach in equalizing the SOC level and assuring constant charging between battery cells. The proposed Switched Quasi Z-source converter is contrasted with the other current topologies, as revealed in Figure 17(a), to find the better voltage gain.

According to the graph, the developed converter outperformed other current techniques, as shown in Table 2, in terms of voltage gain, with a ratio of 1:9. Figure 17 (b) illustrates that the developed converter has high efficiency with the value of 97% compared to other topologies correspondingly.

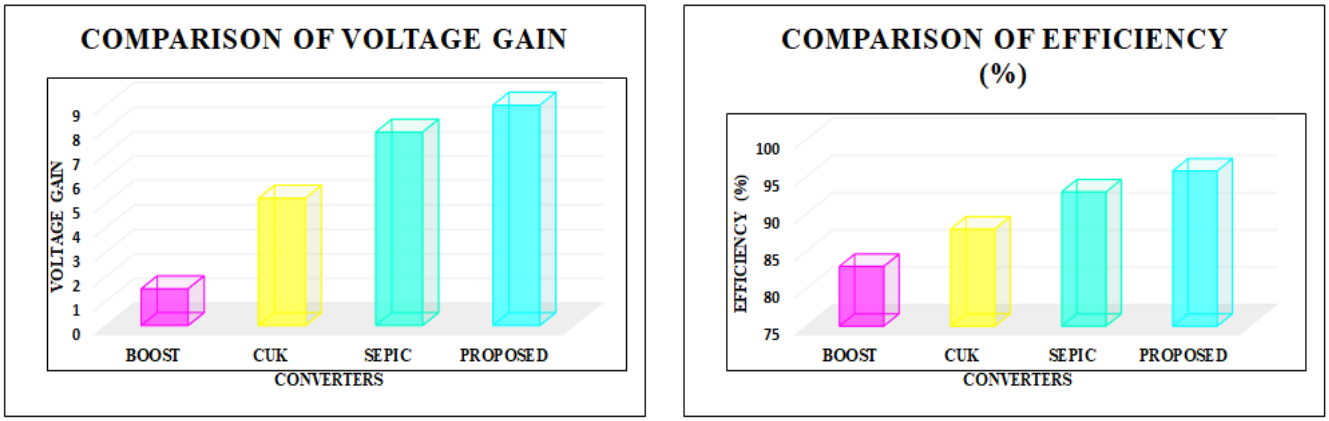

Fig. 17 Comparison of voltage gain

Table 2. Voltage gain comparison

Converters	Voltage gain
Boost [8]	1.5
Cuk[8]	5.2
Sepic[8]	7.9
Proposed	9

Table 3. Comparison of tracking efficiency

Controllers	Tracking efficiency (%)
Fuzzy [9]	94%
ANN [10]	97.64%
ANFIS [11]	98.87%
RBFNN	98.96%

The tracking efficacy of the developed controller is contrasted with that of conventional controllers like fuzzy, ANN, and ANFIS in Table 3. The analysis demonstrates that the proposed RBFNN controller outperforms other current techniques with a greater tracking efficiency of 98.96%.

Figure 18 illustrates an analysis of voltage stress on the switch for Quadratic boost [28], Non-inverted high gain [29], high step-up [30] and developed converter. The Quadratic Boost Converter preserves the lowest and nearly steady voltage stress across the range of voltage gain, representing minimal stress on the switch. In contrast, the Non-Inverted High Gain Converter denotes a steep increase in voltage stress as the voltage gain increases. The High Step Up converter has moderate voltage stress, gradually increasing with the voltage gain. The developed converter attains a balance, posing significantly lower voltage stress compared to the Non-Inverted High Gain and High Step-Up converters, while providing maximum voltage gain. The switch voltage stress for the developed converter increases and remains well below 15, even at high voltage gains. The developed converter efficiently reduces switch voltage stress while attaining high voltage gain.

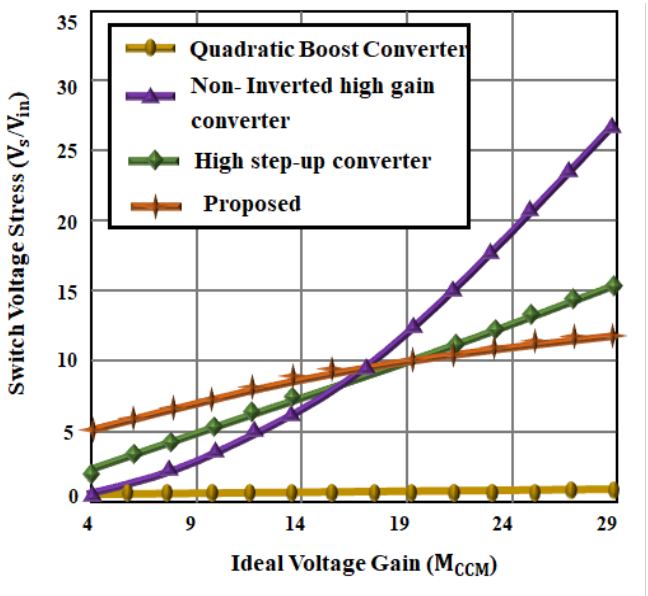

Fig. 18 Comparison of voltage stress

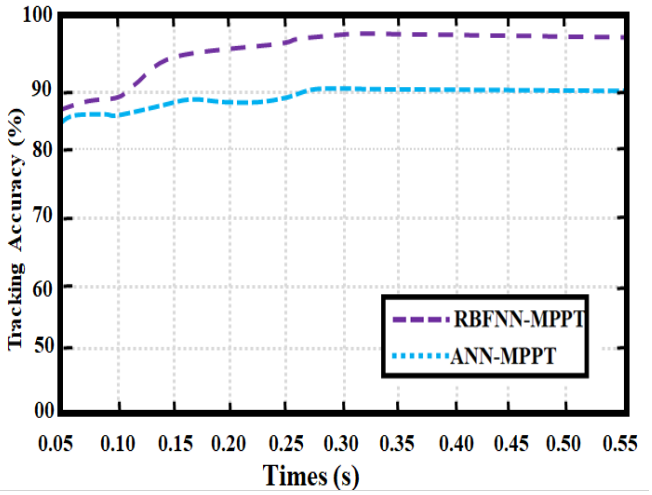

Fig. 19 Analysis of tracking accuracy

Figure 19 illustrates an analysis of tracking accuracy for ANN and the developed MPPT approach, which has the highest tracking accuracy of 97% , thereby assuring the highest tracking power. Parameters like temperature, irradiance and Battery SOC are changed to evaluate the robustness of the Switched Quasi Z-source converter and RBFNN-MPPT controller. The analysis revealed that the system sustains constant voltage regulation, tracking efficiency and load support under changing conditions. Slight deviations in the input of the PV system or Battery SOC had a small influence on output performance, indicating strong adaptability. It assures the resilience and reliability of the developed system in real-world dynamic environments.

4. Conclusion

This research proposes a method for analysing a quasi-Z-source converter with an active balancing circuit in PV-based EV applications. The Switched Quasi Z-Source converter effectively enhances the low voltage, assuring a reliable energy supply for EVs. The developed converter attains a maximum efficacy of 97% and a voltage gain of 1:9. Moreover, the RBFNN-based MPPT topology effectively tracks the optimal power with the greatest tracking efficiency. On the other hand, during an unavailable load supply from the PV system, a battery system is implemented, which distributes power to the load efficiently. The voltage is boosted or lowered via a bi-directional balancing circuit based on the Battery's needs, and it is controlled by a PI controller.

MATLAB/Simulink is employed to implement the proposed work, and the outcomes prove that the developed balancing technique attains lower switching loss during the equalization period, in addition to improving the performance of bidirectional battery equalization with 70% of SOC. At last, comparative analysis is generated over conventional topologies to illustrate the proficiency of the proposed work, which illustrates that the RBFNN-MPPT method has a high tracking efficacy of 98% and the uninterruptible power supply is delivered to the load applications. It promotes sustainable transportation and aids the transition toward clean, decentralized energy systems. However, the efficacy of RBFNN-MPPT severely depends on the quality and diversity of training data, which is not generalised well to temperature and irradiance conditions. Furthermore, while the bidirectional balancing circuit improves battery performance, it introduces extra control complexity.

References

[1] Haseeb Yaqoob et al., "Energy Evaluation and Environmental Impact Assessment of Transportation Fuels in Pakistan," *Case Studies in Chemical and Environmental Engineering*, vol. 3, 2021. [CrossRef] [Google Scholar] [Publisher Link]

[2] Debabrata Mazumdar et al., "GAO Optimized Sliding Mode based Reconfigurable Step Size Pb&O MPPT Controller with Grid Integrated EV Charging Station," *IEEE Access*, vol. 12, pp. 10608-10620, 2024. [CrossRef] [Google Scholar] [Publisher Link]

[3] Subhasish Deb et al., "Charging Coordination of Plug-in Electric Vehicle for Congestion Management in Distribution System Integrated with Renewable Energy Sources," *IEEE Transactions on Industry Applications*, vol. 56, no. 5, pp. 5452-5462, 2020. [CrossRef] [Google Scholar] [Publisher Link]

[4] Noureddine Lasla et al., "Blockchain based Trading Platform for Electric Vehicle Charging in Smart Cities," *IEEE Open Journal of Intelligent Transportation Systems*, vol. 1, pp. 80-92, 2020. [CrossRef] [Google Scholar] [Publisher Link]

[5] Alpaslan Demirci et al., "A Novel Electric Vehicle Charging Management with Dynamic Active Power Curtailment Framework for PV-Rich Prosumers," *IEEE Access*, vol. 12, pp. 120239-120249, 2024. [CrossRef] [Google Scholar] [Publisher Link]

[6] Recep Çakmak, Gökay Bayrak, and Mehmet Koç, "A Fuzzy Logic-Based Energy Management Approach for Fuel Cell and Photovoltaic Powered Electric Vehicle Charging Station in DC Microgrid Operations," *IEEE Access*, vol. 13, pp. 49905-49921, 2025. [CrossRef] [Google Scholar] [Publisher Link]

[7] K. Arulvendhan et al., "Hybrid Compensation based Efficient Wireless Charging System Design with Solar Photovoltaic Interface Toward Sustainable Transportation," *IEEE Access*, vol. 12, pp. 87152-87166, 2024. [CrossRef] [Google Scholar] [Publisher Link]

[8] G. Vasumathi, V. Jayalakshmi, and K. Sakthivel, "Efficiency Analysis of Grid Tied PV System with KY Integrated SEPIC Converter," *Measurement: Sensors*, vol. 27, 2023. [CrossRef] [Google Scholar] [Publisher Link]

[9] Javed Ahmad et al., "Performance Analysis and Hardware-in-the-Loop (HIL) Validation of Single Switch High Voltage Gain DC-DC Converters for MPP Tracking in Solar PV System," *IEEE Access,* vol. 9, pp. 48811-48830, 2020. [CrossRef] [Google Scholar] [Publisher Link]

[10] P. Anbarasan et al., "Performance Enhancement of Grid Integrated Photovoltaic System Using Luo Converter," *IEEE Canadian Journal of Electrical and Computer Engineering,* vol. 45, no. 3, pp. 293-302, 2022. [CrossRef] [Google Scholar] [Publisher Link]

[11] K.S. Kavin, and P. Subha Karuvelam, "PV-Based Grid Interactive PMBLDC Electric Vehicle with High Gain Interleaved DC-DC SEPIC Converter," *IETE Journal of Research*, vol. 69, no. 7, pp. 4791-4805, 2023. [CrossRef] [Google Scholar] [Publisher Link]

[12] Ramin Rahimi et al., "A High Step-Up Z-Source DC-DC Converter for Integration of Photovoltaic Panels into DC Microgrid," *2021 IEEE Applied Power Electronics Conference and Exposition (APEC)*, Phoenix, AZ, USA, pp. 1416-1420, 2021. [CrossRef] [Google Scholar] [Publisher Link]

[13] Abdelkhalek Chellakhi et al., "An Efficient Implementation of Three-Level Boost Converter with Capacitor Voltage Balancing for an Advanced MPPT Approach in PV Systems," *e-Prime-Advances in Electrical Engineering, Electronics and Energy*, vol. 9, 2024. [CrossRef] [Google Scholar] [Publisher Link]

[14] Mazen Yeselam Baramadeh, Mohamed Abd Almonem Abouelela, and Saad Mubarak Alghuwainem "Maximum Power Point Tracker Controller using Fuzzy Logic Control with Battery Load for Photovoltaics Systems," *Smart Grid and Renewable Energy*, vol. 12, no. 10, pp. 163-181, 2021. [CrossRef] [Google Scholar] [Publisher Link]

[15] Karima Et-torabi, and Abdelouahed Mesbahi, "MPPT Based Artificial Neural Network Versus Pertub & Observe for Photovoltaic Energy Conversion System," *E3S Web of Conferences*, vol. 336, pp. 1-6, 2022. [CrossRef] [Google Scholar] [Publisher Link]

[16] Abdullah M. Noman, Khaled E. Addoweesh, and Abdulrahman I. Alolah, "Simulation and Practical Implementation of ANFIS-Based MPPT Method for PV Applications using Isolated Ćuk Converter," *International journal of Photoenergy*, vol. 2017, no. 1, pp. 1- 15, 2017. [CrossRef] [Google Scholar] [Publisher Link]

[17] Surabhi Chandra, and Prerna Gaur, "Radial basis Function Neural Network Technique for Efficient Maximum Power Point Tracking in Solar Photo-Voltaic System," *Procedia Computer Science*, vol. 167, pp. 2354-2363, 2020. [CrossRef] [Google Scholar] [Publisher Link]

[18] Premkumar Manoharan et al., "Improved Perturb and Observation Maximum Power Point Tracking Technique for Solar Photovoltaic Power Generation Systems," *IEEE Systems Journal*, vol. 15, no. 2, pp. 3024-3035, 2020. [CrossRef] [Google Scholar] [Publisher Link]

[19] Ugur Akyol, Dinçer Akal, and Ahmet Durak, "Estimation of Power Output and Thermodynamic Analysis of Standard and Finned Photovoltaic Panels," *Energy Sources, Part A: Recovery, Utilization, and Environmental Effects*, vol. 45, no. 3, pp.8438-8457, 2023. [CrossRef] [Google Scholar] [Publisher Link]

[20] Pedro J. Freire et al., "Performance Versus Complexity Study of Neural Network Equalizers in Coherent Optical Systems," *Journal of Lightwave Technology*, vol. 39, no. 19, pp. 6085-6096, 2021. [Google Scholar] [Publisher Link]

[21] Joel Alpízar-Castillo et al., "Open-Access Model of a PV-BESS System: Quantifying Power and Energy Exchange for Peak-Shaving and Self-Consumption Applications," *Energies,* vol. 16, no. 14, pp. 1-16, 2023. [CrossRef] [Google Scholar] [Publisher Link]

[22] Xiayue Fan et al., "Battery Technologies for Grid-Level Large-Scale Electrical Energy Storage," *Transactions of Tianjin University*, vol. 26, no. 2, pp. 92-103, 2020. [CrossRef] [Google Scholar] [Publisher Link]

[23] Wei Liu, Yan Xu, and Xue Feng, "A Hierarchical and Flexible Data-Driven Method for Online State-of-Health Estimation of Li-Ion Battery," *IEEE Transactions on Vehicular Technology*, vol. 69, no. 12, pp. 14739-14748, 2020. [CrossRef] [Google Scholar] [Publisher Link]

[24] Dongxu Shen et al., "Detection and Quantitative Diagnosis of Micro-Short-Circuit Faults in Lithium-Ion Battery Packs Considering Cell Inconsistency," *Green Energy and Intelligent Transportation*, vol. 2, no. 5, pp. 100-109, 2023. [CrossRef] [Google Scholar] [Publisher Link]

[25] Marco Ragone et al., "Data Driven Estimation of Electric Vehicle Battery State-of-Charge Informed by Automotive Simulations and Multi-Physics Modeling," *Journal of Power Sources*, vol. 483, 2021. [CrossRef] [Google Scholar] [Publisher Link]

[26] Muhammad Uzair, Ghulam Abbas, and Saleh Hosain, "Characteristics of Battery Management Systems of Electric Vehicles with Consideration of the Active and Passive Cell Balancing Process," *World Electric Vehicle Journal*, vol. 12, no. 3, pp. 120, 2021. [CrossRef] [Google Scholar] [Publisher Link]

[27] Micheal A. William et al., "Building Envelopes Toward Energy - Efficient Buildings: A Balanced Multi - Approach Decision Making," *International Journal of Energy Research*, vol. 45, no. 15, pp. 21096-21113, 2021. [CrossRef] [Google Scholar] [Publisher Link]

[28] Guanlin Li, "A Novel Quadratic Boost Converter with Low Inductor Currents," *CPSS Transactions on Power Electronics and Applications*, vol. 5, no. 1, pp. 1-10, 2020. [CrossRef] [Google Scholar] [Publisher Link]

[29] Arshad Mahmood et al., "A Non-Inverting High Gain DC-DC Converter with Continuous Input Current," *IEEE Access*, vol. 9, pp. 54710-54721, 2021. [CrossRef] [Google Scholar] [Publisher Link]

[30] Kazem Varesi, and Naser Hassanpour, Saeid Saeidabadi, "Novel High Step-Up DC-DC Converter with Increased Voltage Gain Per Devices and Continuous Input Current Suitable for DC Microgrid Applications," *International Journal of Circuit Theory and Applications*, vol. 48, 2020. [CrossRef] [Google Scholar] [Publisher Link]